Influences of Conductor Positions and Fast Rising Impulse Voltages on the Line-End Coil based on a Three-Phase High-Frequency Model

Ting Helmholdt-Zhu[1], Volker Grabs[2]

[1] Leibniz University Hannover
Welfengarten 1
30167 Hannover, Germany
helmholdt-zhu@stud.uni-hannover.de

[2] Lenze SE
Hans-Lenze-Straße 1
31855 Aerzen, Germany
volker.grabs@lenze.com

Acknowledgments

The work presented in this publication was supported by the research project UmSiChT, funded by the German Federal Ministry of Education and Research (BMBF). The responsibility for the content of this publication lies with the authors.

Keywords

≪Design optimization≫, ≪Electrical machine≫, ≪Genetic algorithm≫, ≪Pulse Width Modulation (PWM)≫, ≪Wide bandgap devices≫.

Abstract

Due to the steep-edged voltage impulses from the new generation of power electronics, the lifespan of stator insulation systems is significantly shortened. In this paper, a three-phase high-frequency (HF) model based on multi-conductor transmission line theories (MTLs) is developed to predict the electrical field distributions of each conductor in the line-end coils. In addition, the results of possible best and worst conductor spatial distributions in the stator slot from the one-phase HF model on the basis of genetic algorithms are also further investigated by the three-phase HF model. Finally, the theoretical results are validated through partial discharge measurements.

1. Introduction

One of the common failures in electrical machines are the turn-to-turn and turn-to-ground insulation breakdown [1, 2]. The recent trends of wide bandgap devices in power electronics, which switch faster than silicon devices and therefore cause higher inter-turn stress [3, 4], result in a more vulnerable dielectric strength between conductors and the conductor to ground in the line-end coils. Hence, in order to prevent an early malfunction, [5] introduces a one-phase HF model utilizing genetic algorithms (GAs) [6] to investigate the influences of stator conductor spatial positions and rise times of the steep-edged voltage impulses on the transient voltage distributions. However, under real operation conditions the electrical machines are usually supplied by three-phase impulse voltages from an inverter. Therefore, in this paper, the one-phase HF model is further developed to represent a three-phase machine. Comparisons between measured and simulated results through phase current and differential voltage (between phase V and the star point) are demonstrated to validate the three-phase model. Utilizing this validated model, the voltage distributions according to [5] are calculated and compared to the results of the one-phase model. Finally, the simulated outcomes are further validated via partial discharge measurements.

2. Three-Phase High-Frequency Model

The derivation of the three-phase model consists of three main steps [7]: voltage terminal condition, current terminal condition and star point terminal condition. Each step is served to eliminate redundant

variables and information, so that the matrix equations contain only the unknown variables (node voltages of each conductor and three-phase input currents). The following sections start with the introduction of the one-phase model in detail and then further develop it into a three-phase electrical stator winding model.

2.1 One-Phase Model

A stator coil model needs to be separated into two distinct regions: the slot and the overhang (OV) regions due to different distributions of electrical and magnetic fields. Hence, the stator coil can be considered as five discontinuous sections [8], which are interconnected. In other words, there are no mutual coupling among these five sections [9]. Each section is implemented as a MTL [10] and analyzed through the 2n-port network. The admittance parameters ($\boldsymbol{Y}$-parameters) are utilized to describe the network.

A one-phase model, for instance, is presented in Fig. 1, which has 2 coil groups and each coil group occupies two 3-turn coils. The mutual capacitance coupling in OV region between adjacent coils within the same coil group is considered. In order to simplify the HF model, some assumptions are made: the conductor spatial distribution for all slots are the same, thus, for different coils the admittance parameters ($\boldsymbol{Y}$-parameters) are the same; the conductors are positioned parallel against each other and with uniform cross section. Taking this simplified model as an example, the one-phase model of coil group 1 is thus

$$
\begin{bmatrix}
\boldsymbol{I}_{s1}^{1} \\ \boldsymbol{I}_{s2}^{1} \\ -\boldsymbol{I}_{r1}^{1} \\ -\boldsymbol{I}_{r2}^{1} \\ \cdots\cdots \\
\boldsymbol{I}_{s1}^{2} \\ -\boldsymbol{I}_{r1}^{2} \\ \cdots\cdots \\
\boldsymbol{I}_{s2}^{2} \\ -\boldsymbol{I}_{r2}^{2} \\ \cdots\cdots \\
\boldsymbol{I}_{s1}^{3} \\ \boldsymbol{I}_{s2}^{3} \\ -\boldsymbol{I}_{r1}^{3} \\ -\boldsymbol{I}_{r2}^{3} \\ \cdots\cdots \\
\boldsymbol{I}_{s1}^{4} \\ -\boldsymbol{I}_{r1}^{4} \\ \cdots\cdots \\
\boldsymbol{I}_{s2}^{4} \\ -\boldsymbol{I}_{r2}^{4} \\ \cdots\cdots \\
\boldsymbol{I}_{s1}^{5} \\ \boldsymbol{I}_{s2}^{5} \\ -\boldsymbol{I}_{r1}^{5} \\ -\boldsymbol{I}_{r2}^{5}
\end{bmatrix}_{60\times 1}
=
\begin{bmatrix}
\frac{1}{2}\boldsymbol{Y}_{\mathrm{OV}} & & & & & & & & & \\
& \boldsymbol{Y}_{\mathrm{Slot}} & & & & & & & & \\
& & \boldsymbol{Y}_{\mathrm{Slot}} & & & & & & & \\
& & & \boldsymbol{Y}_{\mathrm{OV}} & & & & & & \\
& & & & \boldsymbol{Y}_{\mathrm{Slot}} & & & & & \\
& & & & & \boldsymbol{Y}_{\mathrm{Slot}} & & & & \\
& & & & & & \frac{1}{2}\boldsymbol{Y}_{\mathrm{OV}}
\end{bmatrix}_{60\times 60}
\begin{bmatrix}
\boldsymbol{U}_{s1}^{1} \\ \boldsymbol{U}_{s2}^{1} \\ \boldsymbol{U}_{r1}^{1} \\ \boldsymbol{U}_{r2}^{1} \\ \cdots\cdots \\
\boldsymbol{U}_{s1}^{2} \\ \boldsymbol{U}_{r1}^{2} \\ \cdots\cdots \\
\boldsymbol{U}_{s2}^{2} \\ \boldsymbol{U}_{r2}^{2} \\ \cdots\cdots \\
\boldsymbol{U}_{s1}^{3} \\ \boldsymbol{U}_{s2}^{3} \\ \boldsymbol{U}_{r1}^{3} \\ \boldsymbol{U}_{r2}^{3} \\ \cdots\cdots \\
\boldsymbol{U}_{s1}^{4} \\ \boldsymbol{U}_{r1}^{4} \\ \cdots\cdots \\
\boldsymbol{U}_{s2}^{4} \\ \boldsymbol{U}_{r2}^{4} \\ \cdots\cdots \\
\boldsymbol{U}_{s1}^{5} \\ \boldsymbol{U}_{s2}^{5} \\ \boldsymbol{U}_{r1}^{5} \\ \boldsymbol{U}_{r2}^{5}
\end{bmatrix}_{60\times 1}
\tag{1}
$$

where

- $\boldsymbol{I}_{si}^{j}, -\boldsymbol{I}_{ri}^{j}, \boldsymbol{U}_{si}^{j}$ and $\boldsymbol{U}_{ri}^{j}$ are $(N\times 1)$ current and voltage vectors at sending as well as receiving ends of line. The parameter N indicates the number of turns per coil and in this case, it is equal to 3. The variable $i = 1,2$ presents the number of coils of coil group 1, $j = 1,2,...,5$, according to the five sec-

tions. For example, $\boldsymbol{I}^1_{s1}=[I^1_{s1,1},I^1_{s1,2},I^1_{s1,3}]^T$, $\boldsymbol{I}^1_{r1}=[I^1_{r1,1},I^1_{r1,2},I^1_{r1,3}]^T$ and $\boldsymbol{U}^1_{s1}=[U^1_{s1,1},U^1_{s1,2},U^1_{s1,3}]^T$, $\boldsymbol{U}^1_{r1}=[U^1_{r1,1},U^1_{r1,2},U^1_{r1,3}]^T$.

- $[\boldsymbol{Y}]$ is the admittance matrix of dimension $(10CN \times 10CN)$, and the number 10 comes from 2×5, as there are five sections and each section has the same number of sending and receiving variables, C is the number of coil per coil group and here it is equal to 2. Thus, the dimension of $[\boldsymbol{Y}]$ for this simplified example is (60×60). The definition and calculation of matrices $\boldsymbol{Y}_{OV}$, $\boldsymbol{Y}_{Slot}$ are demonstrated in [8].

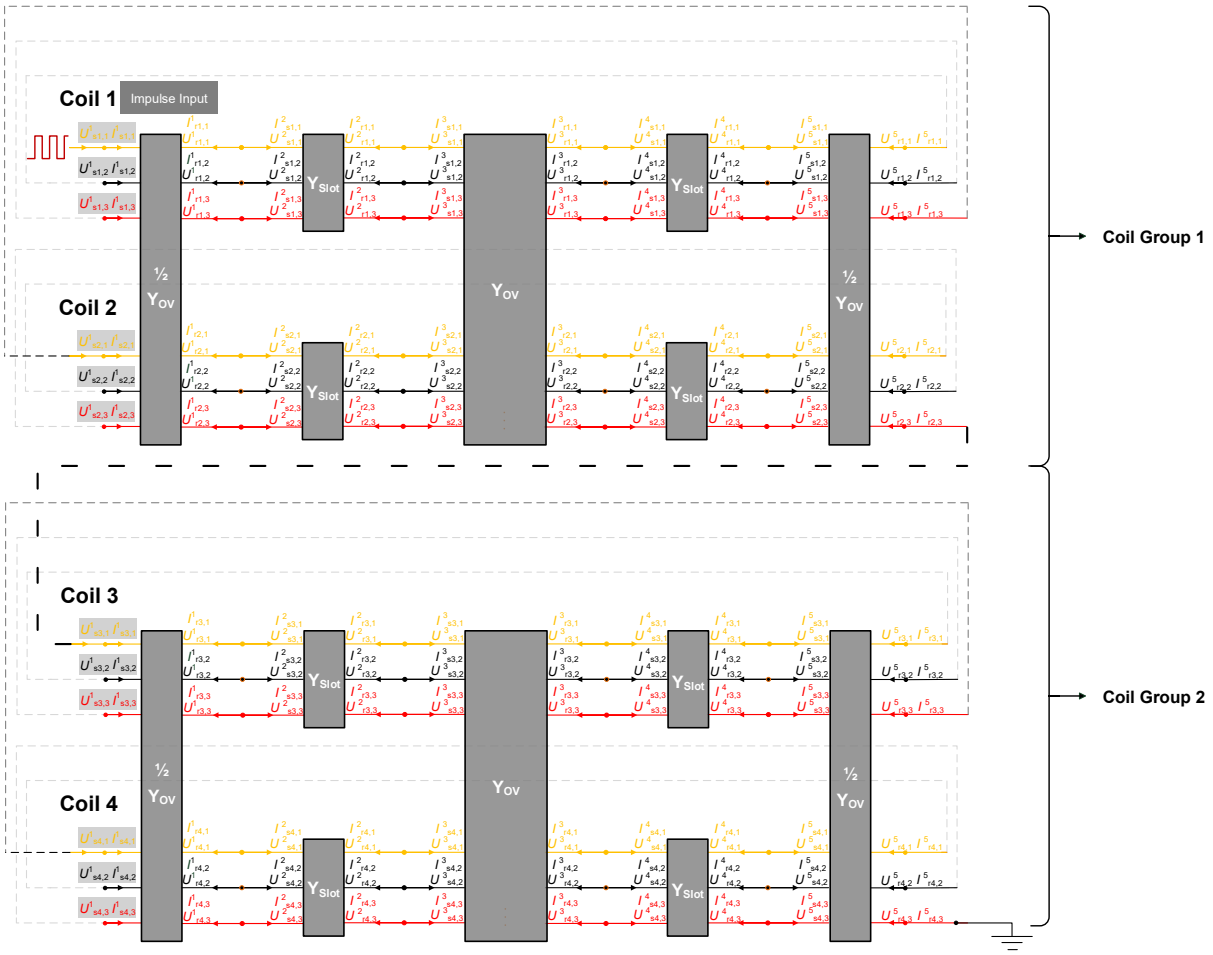

Fig. 1: Example of a one-phase model

Then, Eq. 1 can be summarized as

$$\left[\ \boldsymbol{I}_{C1}\ \right]_{60\times 1}=[\boldsymbol{Y}]_{60\times 60}\left[\ \boldsymbol{U}_{C1}\ \right]_{60\times 1} \tag{2}$$

where C1 indicates the coil group 1. Hence, the result for the whole phase is

$$\begin{bmatrix}\boldsymbol{I}_{C1}\\ \boldsymbol{I}_{C2}\end{bmatrix}=\begin{bmatrix}[\boldsymbol{Y}]_{60\times 60} & \\ & [\boldsymbol{Y}]_{60\times 60}\end{bmatrix}\begin{bmatrix}\boldsymbol{U}_{C1}\\ \boldsymbol{U}_{C2}\end{bmatrix} \tag{3}$$

and C2 indicates the coil group 2, $\boldsymbol{I}_{C1}=[\boldsymbol{I}^1_{s1},\boldsymbol{I}^1_{s2},\cdots,-\boldsymbol{I}^5_{r1},-\boldsymbol{I}^5_{r2}]^T$, $\boldsymbol{I}_{C2}=[\boldsymbol{I}^1_{s3},\boldsymbol{I}^1_{s4},\cdots,-\boldsymbol{I}^5_{r3},-\boldsymbol{I}^5_{r4}]^T$ and $\boldsymbol{U}_{C1}=[\boldsymbol{U}^1_{s1},\boldsymbol{U}^1_{s2},\cdots,\boldsymbol{U}^5_{r1},\boldsymbol{U}^5_{r2}]^T$, $\boldsymbol{U}_{C2}=[\boldsymbol{U}^1_{s3},\boldsymbol{U}^1_{s4},\cdots,\boldsymbol{U}^5_{r3},\boldsymbol{U}^5_{r4}]^T$.

2.1.1 Voltage Terminal Condition

As mentioned, Eq. 3 can be simplified through terminal conditions. The first step is utilizing the voltage terminal condition. Figure 1 shows, that the receiving and sending node voltages between adjacent

sections provide the same information, for instance, $\boldsymbol{U}^1_{\mathrm{r1}}$ and $\boldsymbol{U}^2_{\mathrm{s1}}$, $\boldsymbol{U}^2_{\mathrm{r1}}$ and $\boldsymbol{U}^3_{\mathrm{s1}}$, $\boldsymbol{U}^1_{\mathrm{r2}}$ and $\boldsymbol{U}^2_{\mathrm{s2}}$ etc., thus the receiving parameters can be considered as redundant information and be eliminated. The voltage vector $\begin{bmatrix} \boldsymbol{U}_{\mathrm{C1}} \\ \boldsymbol{U}_{\mathrm{C2}} \end{bmatrix}_{120\times1}$ is reduced to

$$\begin{bmatrix} \boldsymbol{U}_{\mathrm{C1,New}} \\ \cdots\cdots \\ \boldsymbol{U}_{\mathrm{C2,New}} \\ \cdots\cdots \\ U_{\mathrm{end}} \end{bmatrix}_{(60+1)\times1} = \begin{bmatrix} \boldsymbol{U}^1_{\mathrm{s1}/2} \\ \boldsymbol{U}^2_{\mathrm{s1}/2} \\ \boldsymbol{U}^3_{\mathrm{s1}/2} \\ \boldsymbol{U}^4_{\mathrm{s1}/2} \\ \boldsymbol{U}^5_{\mathrm{s1}/2} \\ \cdots\cdots \\ \boldsymbol{U}^1_{\mathrm{s3}/4} \\ \boldsymbol{U}^2_{\mathrm{s3}/4} \\ \boldsymbol{U}^3_{\mathrm{s3}/4} \\ \boldsymbol{U}^4_{\mathrm{s3}/4} \\ \boldsymbol{U}^5_{\mathrm{s3}/4} \\ \cdots\cdots \\ U^5_{\mathrm{r4,3}} \end{bmatrix}_{(60+1)\times1} \tag{4}$$

where U_{end} is the end terminal voltage. In this model it is equal to $U^5_{\mathrm{r4,3}}$ (see Fig. 1). The corresponding transformation matrix is $[\boldsymbol{T}_U]$.

2.1.2 Current Terminal Condition

Similarly, the same approach is carried out for the current vector $\begin{bmatrix} \boldsymbol{I}_{\mathrm{C1}} \\ \boldsymbol{I}_{\mathrm{C2}} \end{bmatrix}_{120\times1}$ to cancel out the sending parameters. As the sending and receiving parameters are opposite in sign, after the addition the sending parameters are equal to 0 and the corresponding transformation matrix is $[\boldsymbol{T}_I]$. Afterwards, the current vector is further simplified by eliminating the receiving parameters, as they are redundant information. The final current vector is thus

$$\begin{bmatrix} \boldsymbol{I}_{\mathrm{C1,New}} \\ \cdots\cdots \\ \boldsymbol{I}_{\mathrm{C2,New}} \\ \cdots\cdots \\ -I_{\mathrm{end}} \end{bmatrix}_{(60+1)\times1} = \begin{bmatrix} I^1_{\mathrm{s1,1}} \\ \vdots \\ 0 \\ \cdots\cdots \\ 0 \\ \vdots \\ 0 \\ \cdots\cdots \\ -I^5_{\mathrm{r4,3}} \end{bmatrix}_{(60+1)\times1} \tag{5}$$

The transformation matrix is $[\boldsymbol{T}_{\mathrm{I,Eli}}]$.

2.2 Three-Phase Model

After the simplification of voltage and current terminal conditions, the expression of Eq. 3 is modified as

$$\begin{bmatrix} \boldsymbol{I}_{\mathrm{C1,New}} \\ \cdots\cdots \\ \boldsymbol{I}_{\mathrm{C2,New}} \\ \cdots\cdots \\ -I_{\mathrm{end}} \end{bmatrix}_{(60+1)\times1} = [\boldsymbol{Y}_{\mathrm{Mod}}] \begin{bmatrix} \boldsymbol{U}_{\mathrm{C1,New}} \\ \cdots\cdots \\ \boldsymbol{U}_{\mathrm{C2,New}} \\ \cdots\cdots \\ U_{\mathrm{end}} \end{bmatrix}_{(60+1)\times1} \tag{6}$$

where $[\boldsymbol{Y}_{\text{Mod}}]$ is the modified admittance matrix

$$[\boldsymbol{Y}_{\text{Mod}}]_{(60+1)\times(60+1)} = \underbrace{[\boldsymbol{T}_{\text{I,Eli}}]_{(60+1)\times 120}\big(\underbrace{[\boldsymbol{T}_{\text{I}}]_{120\times 120}\big(\overbrace{[\boldsymbol{Y}]_{120\times 120}[\boldsymbol{T}_{\text{U}}]_{120\times(60+1)}}^{\text{Voltage Terminal Condition}}\big)}_{\text{Current Terminal Condition}}\big)}_{\text{Current Terminal Condition}} \tag{7}$$

Based on Eq. 6 and the simplified one-phase model, a three-phase (U, V, W) stator winding is thus

$$\begin{bmatrix} I^1_{\text{sU1,1}} \\ \mathbf{0} \\ \cdots\cdots \\ -I^5_{\text{rU4,3}} \\ \hline I^1_{\text{sV1,1}} \\ \mathbf{0} \\ \cdots\cdots \\ -I^5_{\text{rV4,3}} \\ \hline I^1_{\text{sW1,1}} \\ \mathbf{0} \\ \cdots\cdots \\ -I^5_{\text{rW4,3}} \end{bmatrix} = \begin{bmatrix} [\boldsymbol{Y}_{\text{Mod}}] & & \\ & [\boldsymbol{Y}_{\text{Mod}}] & \\ & & [\boldsymbol{Y}_{\text{Mod}}] \end{bmatrix} \begin{bmatrix} U^1_{\text{sU1,1}} \\ \vdots \\ \cdots\cdots \\ U^5_{\text{rU4,3}} \\ \hline U^1_{\text{sV1,1}} \\ \vdots \\ \cdots\cdots \\ U^5_{\text{rV4,3}} \\ \hline U^1_{\text{sW1,1}} \\ \vdots \\ \cdots\cdots \\ U^5_{\text{rW4,3}} \end{bmatrix} \tag{8}$$

In this paper, the end terminal condition is a star connection: $I^5_{\text{rU4,3}} + I^5_{\text{rV4,3}} + I^5_{\text{rW4,3}} = 0$ and $U^5_{\text{rU4,3}} = U^5_{\text{rV4,3}} = U^5_{\text{rW4,3}} = U_{\text{UN}}$, where U_{UN} is the star point voltage.

2.2.1 Star-Terminal Connection

Using ($I^5_{\text{rU4,3}} + I^5_{\text{rV4,3}} + I^5_{\text{rW4,3}} = 0$) and ($U^5_{\text{rU4,3}} = U^5_{\text{rV4,3}} = U^5_{\text{rW4,3}} = U_{\text{UN}}$) to further eliminate redundant information of Eq. 8

$$\begin{bmatrix} I^1_{\text{sU1,1}} \\ \mathbf{0} \\ \hline I^1_{\text{sV1,1}} \\ \mathbf{0} \\ \hline I^1_{\text{sW1,1}} \\ \mathbf{0} \\ \cdots\cdots \\ 0 \end{bmatrix} = [\boldsymbol{T}_{\text{I,end}}] \begin{bmatrix} [\boldsymbol{Y}_{\text{Mod}}] & & \\ & [\boldsymbol{Y}_{\text{Mod}}] & \\ & & [\boldsymbol{Y}_{\text{Mod}}] \end{bmatrix} [\boldsymbol{T}_{\text{U,end}}] \begin{bmatrix} U^1_{\text{sU1,1}} \\ \vdots \\ \hline U^1_{\text{sV1,1}} \\ \vdots \\ \hline U^1_{\text{sW1,1}} \\ \vdots \\ \cdots\cdots \\ U_{\text{UN}} \end{bmatrix} \tag{9}$$

where $[\boldsymbol{T}_{\text{I,end}}]$ and $[\boldsymbol{T}_{\text{U,end}}]$ are the corresponding transformation matrices and the new modified admittance matrix is expressed as $[\boldsymbol{Y}'_{\text{Mod}}]$. In order to solve this matrix equation (Eq. 9), the unknown variables (node voltages and three-phase input currents) should be placed in a vector together through the trans-

formation matrices $[\boldsymbol{T}_{\mathrm{Mod,I}}]$ and $[\boldsymbol{T}_{\mathrm{Mod,U}}]$

$$\begin{bmatrix} I^1_{\mathrm{sU1,1}} \\ I^1_{\mathrm{sV1,1}} \\ I^1_{\mathrm{sW1,1}} \\ \cdots\cdots \\ \mathbf{0} \\ \cdots\cdots \\ 0 \end{bmatrix} = [\boldsymbol{T}_{\mathrm{Mod,I}}][\boldsymbol{Y}'_{\mathrm{Mod}}][\boldsymbol{T}_{\mathrm{Mod,U}}] \begin{bmatrix} U^1_{\mathrm{sU1,1}} \\ U^1_{\mathrm{sV1,1}} \\ U^1_{\mathrm{sW1,1}} \\ \cdots\cdots \\ \vdots \\ \cdots\cdots \\ U_{\mathrm{UN}} \end{bmatrix} \tag{10}$$

The new admittance matrix is $[\boldsymbol{Y}''_{\mathrm{Mod}}]$. In the voltage vector, the three input voltages ($U^1_{\mathrm{sU1,1}}$, $U^1_{\mathrm{sU1,1}}$ and $U^1_{\mathrm{sW1,1}}$) are known, thus, the final step is the rearrangement of current and voltage vectors. The matrix $[\boldsymbol{Y}''_{\mathrm{Mod}}]$ is, hence, partitioned into

$$[\boldsymbol{Y}''_{\mathrm{Mod}}] = \left[\begin{array}{c|c} \boldsymbol{Y}''_{\mathrm{Mod,\ 11}} & \boldsymbol{Y}''_{\mathrm{Mod,\ 12}} \\ \hline \boldsymbol{Y}''_{\mathrm{Mod,\ 21}} & \boldsymbol{Y}''_{\mathrm{Mod,\ 22}} \end{array}\right] \tag{11}$$

Now the matrix equation (Eq. 10) is expressed as

$$\left[\begin{array}{c} I^1_{\mathrm{sU1,1}} \\ I^1_{\mathrm{sV1,1}} \\ \hline I^1_{\mathrm{sW1,1}} \\ \\ \mathbf{0} \\ 0 \end{array}\right] = \left[\begin{array}{c|c} \boldsymbol{Y}''_{\mathrm{Mod,\ 11}} & \boldsymbol{Y}''_{\mathrm{Mod,\ 12}} \\ \hline \boldsymbol{Y}''_{\mathrm{Mod,\ 21}} & \boldsymbol{Y}''_{\mathrm{Mod,\ 22}} \end{array}\right] \left[\begin{array}{c} U^1_{\mathrm{sU1,1}} \\ U^1_{\mathrm{sV1,1}} \\ \hline U^1_{\mathrm{sW1,1}} \\ \vdots \\ U_{\mathrm{UN}} \end{array}\right] \tag{12}$$

Moving all the unknown variables (node voltages) in the voltage vector to the left side of the equation

$$\left[\begin{array}{c} I^1_{\mathrm{sU1,1}} \\ I^1_{\mathrm{sV1,1}} \\ \hline I^1_{\mathrm{sW1,1}} \\ \vdots \\ U_{\mathrm{UN}} \end{array}\right] = \left[\begin{array}{c} \boldsymbol{Y}''_{\mathrm{Mod,\ 11}} - \boldsymbol{Y}''_{\mathrm{Mod,\ 12}}(\boldsymbol{Y}''_{\mathrm{Mod,\ 22}})^{-1}\boldsymbol{Y}''_{\mathrm{Mod,\ 21}} \\ \hline -(\boldsymbol{Y}''_{\mathrm{Mod,\ 22}})^{-1}\boldsymbol{Y}''_{\mathrm{Mod,\ 21}} \end{array}\right] \left[\begin{array}{c} U^1_{\mathrm{sU1,1}} \\ U^1_{\mathrm{sV1,1}} \\ \hline U^1_{\mathrm{sW1,1}} \\ \\ \mathbf{0} \\ 0 \end{array}\right] \tag{13}$$

As is shown, the left side of the matrix equation consists of all required unknown variables (input line currents and node voltages of each conductor in each section). At the right side, the modified admittance matrix is known based on the calculation of winding parameters of each conductor [8] and the voltage vector is also known, as the three-phase input voltages are obtained through measurement (illustrated in Section 3). The solving process is based on the fast Fourier transformation (FFT) and inverse-FFT, which is illustrated in [5][8].

3. Model Validation

The mathematical one-phase model is determined through two parts: Methods of determining conductor parameters and the structure of a single-coil model based on MTLs. The validations of these two parts are demonstrated in [8]. For a more complicated three-phase model, it is necessary to conduct further validation measurements.

3.1 Best Case I: Conductor Distribution

According to the results of [5], one of the optimized distributions is, that stator conductors start from the bottom of the slot and spread to the slot opening (for example, see Fig. 2(a)). It is named as 'Best Case I'. With the same distribution an electrical machine is constructed (see Fig. 2(b)(c)).

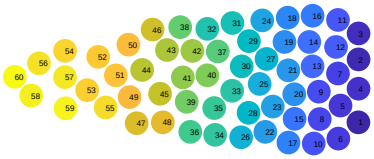

(a) Best Case I: Slot 1[5]

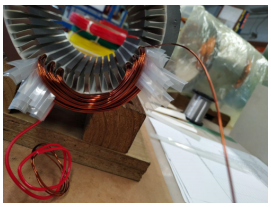

(b) Best Case I distribution for each coil

(c) Separation of the slot in ten layers

Fig. 2: Best Case I electrical machine

Each coil are separated in six groups and each group contains ten conductors. Taking one line-end coil as an example, the first group is turn 1 to turn 10, then turn 11 to turn 20, turn 21 to turn 30, until the last group turn 51 to turn 60. Afterwards, conductors are positioned in the slot according to the group number and each group is separated through a thin film (see Fig. 2(b)(c)), so that conductors in different groups are not mixed to each other. Eventually, these thin films are removed and the electrical machine has a similar conductor distribution as the theoretical optimization results of Best Case I and can be utilized to validate the three-phase HF model according to Eq. 13.

3.2 Model Validation

First of all, the real three-phase impulse voltages ($U^1_{\mathrm{sU1,1}}$, $U^1_{\mathrm{sV1,1}}$ and $U^1_{\mathrm{sW1,1}}$) with a 16 kHz switching frequency from a three-phase silicon carbide (SiC)-based inverter are measured and defined as input values for the three-phase HF model (see Fig. 3).

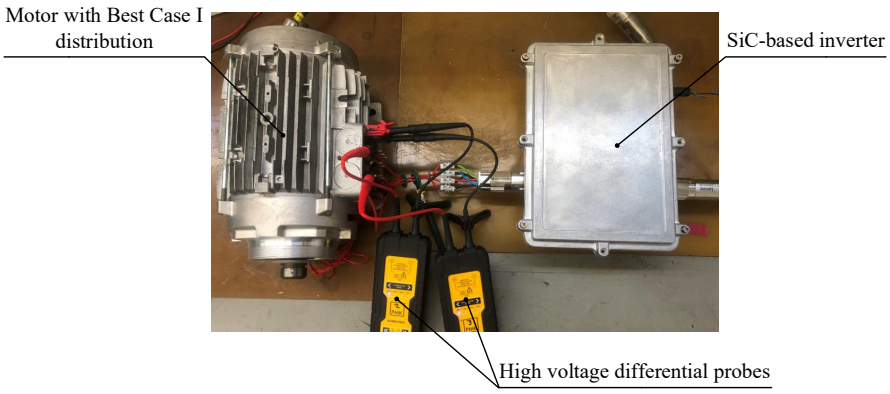

Fig. 3: Three-phase voltages measurement

Besides, the voltages are measured with two different rise times, which is realized through two gate resistances (20 Ω: 55 V/ns, 0.5 Ω: 100 V/ns) of the SiC-based inverter.

3.2.1 Voltage Validation

The differential voltage between phase V (U_{V}) and the star point (U_{UN}) is measured as one of the comparison criterion (see Fig. 4). Using the results from 0.5 Ω, it can be seen, that the simulated and measured differential voltages ($U_{\mathrm{V,\,UN}}$) show a close agreement. The differential voltage ($U_{\mathrm{V,\,UN}}$) oscillates during each switching operation. This is caused by the high-frequency parts contained in the switching edge, which excites the resonance frequency of the parasitic impedance from the conductors.

3.2.1 Current Validation

The phase current measurement is conducted through a current probe from Tektronix TCP0030, which has a bandwidth of 0-120 MHz. Figure 5 shows the measured and calculated current curves by 20 Ω and

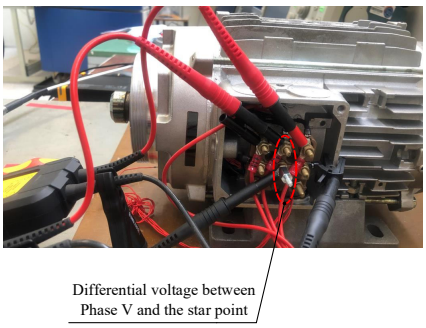

(a) Differential voltage $U_{\mathrm{V,\,UN}}$ measurement

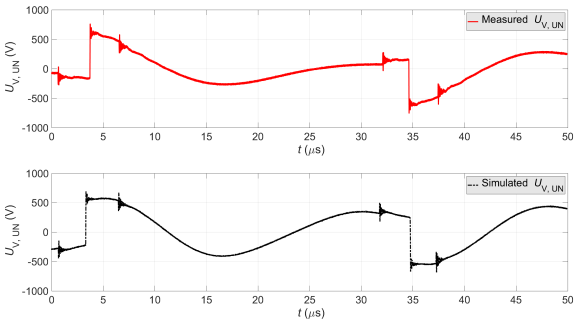

(b) Validation through differential voltage $U_{\mathrm{V,\,UN}}$

Fig. 4: Voltage validation

0.5 Ω of phase U, for instance. In general, both simulated and measured values show the same trend: with decreased gate resistance, the peak amplitude of the current is increased.

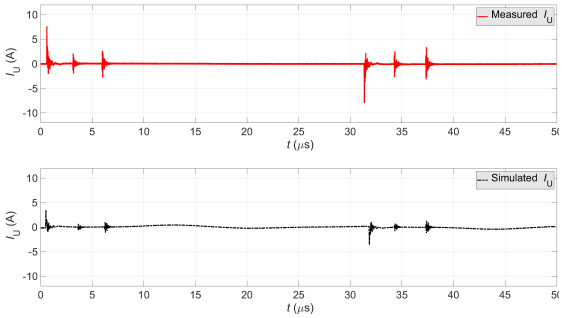

(a) I_{U} at 20 Ω

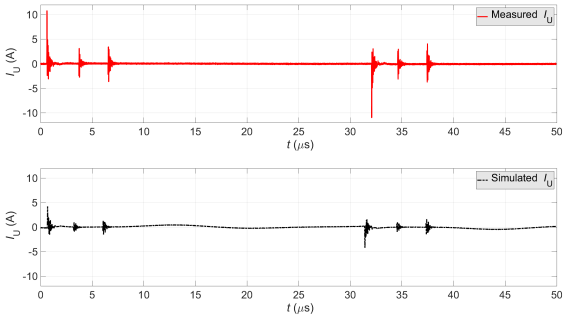

(b) I_{U} at 0.5 Ω

Fig. 5: Current validation

The variation of amplitudes between simulated and measured values is caused by following reasons: firstly, the limitation of the current probe due to the frequency bandwidth; secondly, the interruption from high-frequency noises of the SiC power electronics; thirdly, the exact values of the permittivity from stator insulation materials are unknown. Therefore, a precise prediction of the peak-amplitude is difficult to achieve in terms of both the limited measurement technique and the identifications of accurate material data. However, the purpose of this research is to compare and study the changes of different conductor distributions made on the transient voltage distribution in line-end coils. Therefore, the results can also be compared after a normalization. Using phase current I_{U} at 0.5 Ω as an example (see Fig. 6).

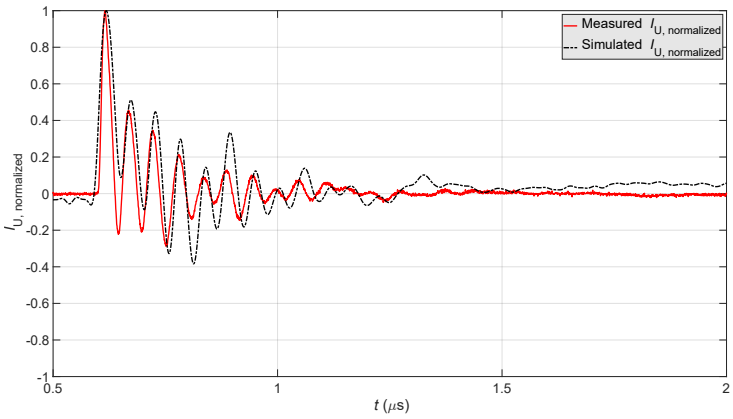

Fig. 6: Normalized phase current I_{U}

As demonstrated, the transient oscillations of measured phase current can be accurately predicted by the simulated results from the three-phase HF model in terms of the curve shape and the transient vibrations.

4. Results from Best and Worst Cases based on the Three-Phase HF Model

The results of field strength in line-end coils based on the three-phase model show the same advantages of utilizing the Best Case II distribution [5] (see Fig. 7(a)) (the other way around than Best Case I, see Fig. 7(a)). The Worst Case [5] indicates, that turn 1 and turn 60 (the last turn) of the line-end coil are placed directly next to each other (see Fig. 7(b)). It is noticeable, that the advantage of Best Case II distribution in terms of the maximum field strength (Fig. 7(b)(c)), which is already illustrated in [5] based on the one-phase HF model, is also validated through a three-phase HF model.

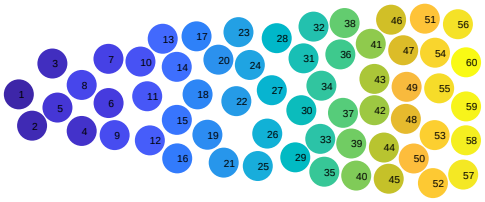

(a) Best Case II: Slot 2[5]

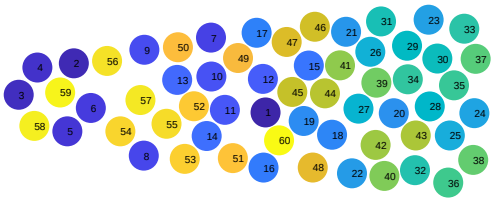

(b) Worst Case: Slot 4[5]

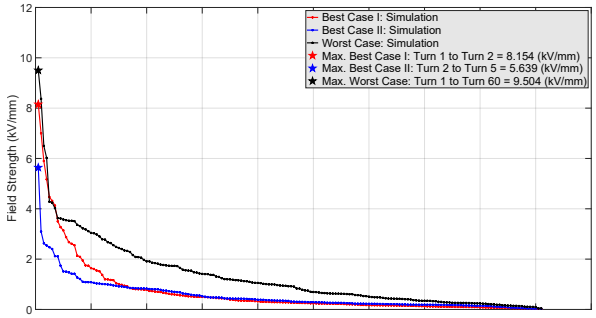

(c) Sorted field strength at 20 Ω

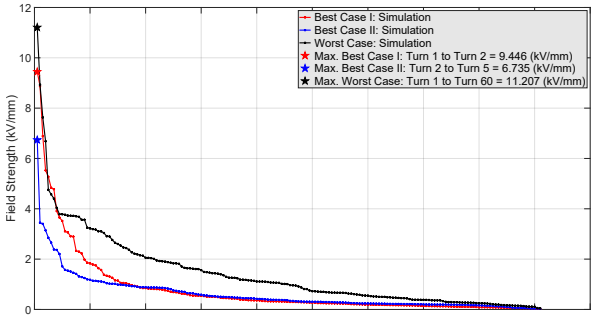

(d) Sorted field strength at 0.5 Ω

Fig. 7: (a) and (b) illustrate conductor distributions of Best Case II and Worst Case. The color presents the turn number from turn 1 (dark blue) to turn 60 (light yellow); (c) and (d) show the sorted field strengths by 20 Ω and 0.5 Ω with Best Case I, II and Worst Case conductor distributions

5. Validation of Best and Worst Cases through Surge Voltage Tests

In order to validate the theoretical results of Best and Worst Cases distributions on the dielectric strength of the stator winding insulation system under impulse voltages, test stators with similar spatial arrangements are constructed (see Fig. 8).

Overall, there are three different types of test stators:

- Type 1: The conductors are distributed randomly, like the nowadays standard serial product.
- Type 2: The line-end coil based on the Worst Case distribution (the first and last turns placed directly next to each other), but with an extra sleeving of the first turn (Fig. 8(a)).
- Type 3: All coils are sorted based on the Best Case II distribution (Fig. 8(b)). In the meantime, with an exchange on the end of the star point, the spatial arrangement of conductors is then the other way around (from Best Case II to Best Case I). At the beginning, the conductors are separated in seven groups using kapton tape in the two OV regions (Fig. 8(b)). The first group (Group 1) contains turn 1 and turn 2. The rest groups have 3 turns each according to the sequence.

All the stators have the same winding topology with three parallel wires of each turn, one layer and three phases with double impregnation. Each version has two test stators, so, in total, there are 6 specimens. The measurement is conducted with the MTC2 surge voltage tester. The applied voltage starts from 2 kV and rises 250 V on each step, which contains 10 impulses. Each phase is tested for turn-turn insulation in

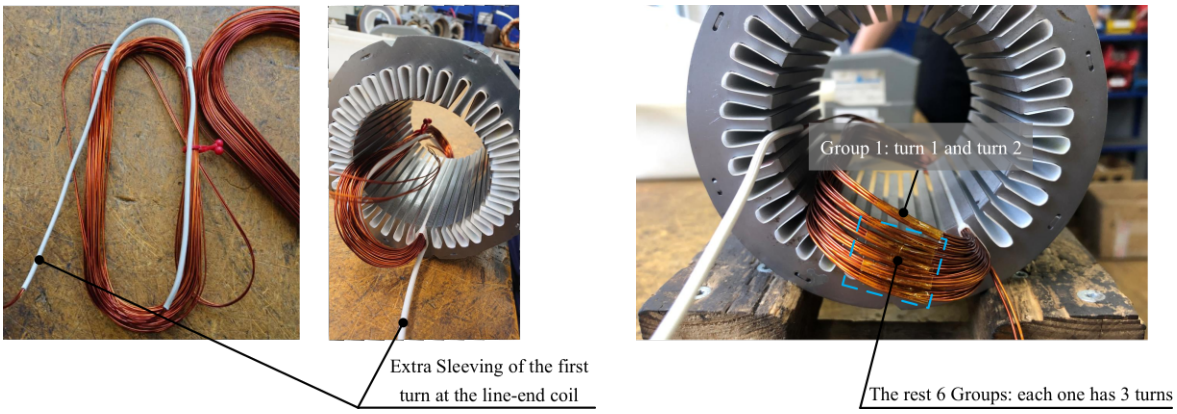

(a) Worst Case: Turn 1 with an extra sleeving (b) Best Case I, II: Sorted conductors of each coil

Fig. 8: Best Case I, Best Case II and Worst Case distributions

terms of the repetitive partial discharge inception voltage (RPDIV) and each test is repeated three times (see Fig. 9).

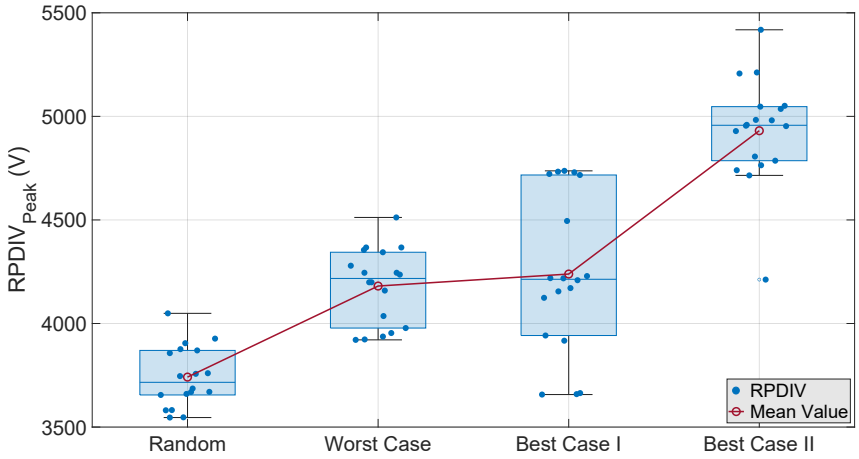

Fig. 9: RPDIV results of four different conductor distributions

As is shown, Best Case II represents an obvious higher inter-turn dielectric strength than Best Case I, Worst Case with an extra sleeving and Random distribution. Based on the mean value of Random distribution (3741.3 V), an enhancement of the RPDIV at Worst Case with an extra sleeving, Best Case I and Best Case II is of around 12 %, 13 % and 32 %, respectively.

5. Conclusion

In this paper, a three-phase HF model is introduced and validated through both voltage and current measurements. Besides, based on this model, the transient voltages along the first coil of each phase are calculated in terms of Best Case I, II and Worst Case distributions, which are the optimized results from one-phase HF model. The outcomes show again, that under Best Case II distribution the maximum value of electric field strength between nearby conductors is being the most restrained.

In addition, there are 6 test stators with different spatial conductor distributions being constructed to further validate the theoretical conclusions and the results show a high agreement: the RPDIV mean value of Best Case II stators are clearly the highest with an increase of 32 % compared to that of Random distributed stators. Furthermore, the advantage of utilizing an extra sleeving of turn 1 under worst case condition is not significantly demonstrated in the partial discharge measurement results. This partial discharge measurement should be further conducted with real SiC-inverters, so that the other effects (for example, the switching frequency, the peak voltage, etc.) can also be studied.

References

[1] D. E. Schump, "Testing to assure reliable operation of electric motors," 34th Annual Conference on Rural Electric Power, 1990, pp. B4/1-B4/6, doi: 10.1109/REPCON.1990.68527

[2] J. Geiman, "DC step-voltage and surge testing of motors", Maint. Technol., vol. 20, no. 3, pp. 3239, 2007

[3] A. Hoffmann and B. Ponick, "Method for the Prediction of the Potential Distribution in Electrical Machine Windings Under Pulse Voltage Stress," in IEEE Transactions on Energy Conversion, vol. 36, no. 2, pp. 1180-1187, June 2021, doi: 10.1109/TEC.2020.3026531

[4] Y. Xie, J. Zhang, F. Leonardi, A. R. Munoz, M. W. Degner and F. Liang, "Modeling and Verification of Electrical Stress in Inverter-Driven Electric Machine Windings," in IEEE Transactions on Industry Applications, vol. 55, no. 6, pp. 5818-5829, Nov.-Dec. 2019, doi: 10.1109/TIA.2019.2937068

[5] T. Helmholdt-Zhu and H. Borcherding, "Investigations on the Influences of Winding Positions and Rise Times on the Winding Isolation System within the Line-End Coil under Fast Rising Impulse Voltages," 2021 23rd European Conference on Power Electronics and Applications (EPE'21 ECCE Europe), 2021, pp. 1-10

[6] Sumathi, S. et al, "Evolutionary Intelligence," 1nd Ed., Springer, 2008

[7] J. L. Guardado and K. J. Cornick, "A computer model for calculating steep-fronted surge distribution in machine windings," in IEEE Transactions on Energy Conversion, vol. 4, no. 1, pp. 95-101, March 1989, doi: 10.1109/60.23156

[8] T. Helmholdt-Zhu, B. Knebusch and H. Borcherding, "High-Frequency Models for the Prediction of Transient Effects in Motor Windings under Fast Rising Impulse Voltages," PCIM Europe digital days 2020; International Exhibition and Conference for Power Electronics, Intelligent Motion, Renewable Energy and Energy Management, 2020, pp. 1-8

[9] B.S. Oyegoke, "Transient Voltage Distribution in Stator Winding of Electrical Machine Fed from a Frequency Converter," Finnish Academies of Technology, 2000

[10] C.R. Paul., "Analysis of Multiconductor Transmission Lines," 2nd. John Wiley & Sons, Inc., 2008